Faraday Discussions
Cite this: *Faraday Discuss.*, 2024, **254**, 216

PAPER

Challenges with relativistic *GW* calculations in solids and molecules

Gaurav Harsha, [a] Vibin Abraham [a] and Dominika Zgid *[ab]

Received 29th February 2024, Accepted 4th March 2024
DOI: 10.1039/d4fd00043a

For molecules and solids containing heavy elements, accurate electronic-structure calculations require accounting not only for electronic correlations but also for relativistic effects. In molecules, relativity can lead to severe changes in the ground-state description. In solids, the interplay between both correlation and relativity can change the stability of phases or it can lead to an emergence of completely new phases. Traditionally, the simplest illustration of relativistic effects can be done either by including pseudopotentials in non-relativistic calculations or alternatively by employing large all-electron basis sets in relativistic methods. By analyzing different electronic properties (band structure, equilibrium lattice constant and bulk modulus) in semiconductors and insulators, we show that capturing the interplay of relativity and electron correlation can be rather challenging in Green's function methods. For molecular problems with heavy elements, we also observe that similar problems persist. We trace these challenges to three major problems: deficiencies in pseudopotential treatment as applied to Green's function methods, the scarcity of accurate and compact all-electron basis sets that can be converged with respect to the basis-set size, and linear dependencies arising in all-electron basis sets, particularly when employing Gaussian orbitals. Our analysis provides detailed insight into these problems and opens a discussion about potential approaches to mitigate them.

I. Introduction

Computational methods in *ab initio* electronic structure theory have become indispensable tools in the design and study of new functional materials and molecules. For many years, mean-field methods such as density functional theory[1,2] (DFT) and Hartree–Fock (HF) were the commonly employed simulation tools mostly due to their low computational cost and reasonable accuracy. However, recently, due to advances in computational resources as well as algorithms, sophisticated methods capturing electronic correlation beyond the mean-field approximation have gathered much more attention. Examples include coupled cluster,[3,4] perturbation theories for wave functions and Green's functions,[5–9] and embedding methods,[10–19] among others.

[a]*Department of Chemistry, University of Michigan, Ann Arbor, Michigan 48109, USA. E-mail: zgid@umich.edu*
[b]*Department of Physics, University of Michigan, Ann Arbor, Michigan 48109, USA*

The development of new electronic structure methods is primarily driven by one or both of the following objectives: (i) accurate description of electron correlation, and (ii) applicability to realistic systems with a large number of electrons. Addressing both of these challenges satisfactorily is usually very difficult. For instance, low-scaling mean-field methods such as DFT and HF (with $\mathcal{O}(N^3)$ and $\mathcal{O}(N^4)$ computational costs, respectively, N being a measure of system size) can be applied to very large systems. However, they often lack quantitative accuracy. On the other hand, coupled cluster with single, double and perturbative triple excitation, *i.e.*, CCSD(T), is considered as the gold standard for description of dynamical correlation, but has limited applicability due to its high $\mathcal{O}(N^7)$ scaling. Consequently, greater recovery of correlation effects usually comes hand-in-hand with an increased computational cost.

The *GW* method,[5,20–22] derived from Hedin's perturbation theory for the single-particle Green's function, offers a reasonable balance between accuracy and cost. In comparison to DFT or HF, it provides a high-level description of correlation effects at a formal scaling of $\mathcal{O}(N^6)$, which is usually brought down to $\mathcal{O}(N^4)$ by using approximations such as the density-fitting procedure.[23–25] The good accuracy of *GW* can be explained by its diagrammatic similarities with theories like coupled cluster and random phase approximation.[26–29] Additionally, *GW* has shown versatility in its application to both finite[30–39] and extended systems.[40–45]

As the applications of computational methods are expanded to systems with heavy elements, another challenge arises: the problem of accurate inclusion of relativity. Even for elements in the third and fourth rows of the periodic table, relativistic effects are important.[46] While for a full relativistic description, the 4-component Dirac equation, instead of the regular non-relativistic Schrödinger equation, should be solved, solving the 4-component equation is a formidable task and not strictly necessary for most systems if only the electronic structure properties are of interest. Several approximations have been proposed to introduce the full relativistic physics into an effective Hamiltonian that describes only the electronic degrees of freedom. The most widely used approximation follows the work of Breit,[47] where the Dirac equation is reduced to a Schrödinger-like equation with an effective Dirac–Coulomb–Breit Hamiltonian that contains the relativistic terms. Theories such as the Douglas–Kroll–Hess[48–52] approach and the exact two-component[53–57] (X2C) theory introduce further approximations to make relativistic calculations achievable. Several *ab initio* implementations for realistic systems of the relativistic *GW* theory have emerged in the condensed matter community,[58–61] and in the quantum chemistry community,[37,62,63] where the latter are based on the X2C Hamiltonian.

Calculations in the X2C approach are generally performed using all-electron basis sets since current pseudopotentials (PPs) or effective core potentials (ECPs) do not recover relativistic effects, such as spin–orbit coupling (SOC). Most modern implementations or *ab initio* relativistic codes are capable of handling relativistic elements, at least up to the 5th or 6th row, including the Lanthanides, in the periodic table. Yet, performing reliable *GW* calculations for accurate electronic structure properties still remains an arduous task. Considering that the *GW* approximation is the simplest in the hierarchy of Hedin's perturbation theory, it offers an understandably limited accuracy in describing electron correlation. However, factors other than the accuracy of the *GW* method, *e.g.*, poor quality and availability of basis sets, lack of effective PPs, *etc.*, can have a larger impact on the quality of results, particularly in heavy elements.

In this discussion article, we analyze the factors that hinder the applicability of the sophisticated machinery of *GW* to both solids and molecules containing heavy elements. In particular, we first highlight the need for all-electron relativistic calculations due to the inability of PPs to account for many important relativistic effects. We then investigate problems with achieving the basis set convergence in *GW* calculations. This is followed by results that highlight linear dependencies arising in larger basis sets. Such problems often aggravate the issue of slow convergence with respect to basis set size. Finally, we also comment on possible improvements of experimental results that are ultimately necessary for benchmarking and validating new theoretical methods. By investigating multiple properties of solids and molecules, we perform a comprehensive analysis of how several external factors, other than the accuracy of the method itself, influence the results in self-consistent *GW* (sc*GW*).

This article is organized as follows: in Section II, we recap some of the theoretical concepts on which the majority of this paper is based. This is followed by computational and implementation details in Section III. In Section IV, we analyze various hurdles, one by one, for the application of sc*GW* to relativistic systems. A general discussion and conclusions on possible factors behind these challenges, along with the current and future developments that can address these problems, is presented in Section V.

II. Methods

In this work, we employ mean-field methods and self-consistent *GW* (sc*GW*) theory within the X2C relativistic formalism.[53–57] While most of the theoretical and implementation details can be found in ref. 39, 63 and 64, here we provide a brief overview of important concepts, namely the relativistic Hamiltonian, sc*GW* theory, and Birch–Murnaghan[65,66] equation of state that we use to study bulk properties in materials. Note that while *GW* by itself[21,40,64,67–73] provide excellent results for weakly correlated compunds, it is also important for embedding approaches[74–80] where it is usually employed as a low-level method for treating the environment.

A. Relativistic Hamiltonian: exact two-component formalism

The X2C formalism is widely used among electronic structure relativistic methods.[55–57,81] In this formalism, the four-component one-body Dirac–Coulomb Hamiltonian H^{4C1e} is used as a starting point on which a unitary transformation is performed that decouples the eigenvectors with large and small eigenvalues, generally labeled as large and small components,

$$\begin{aligned} U^{\dagger}H^{4C1e}U &= U^{\dagger}\begin{bmatrix} \hat{V} & \hat{T} \\ \hat{T} & \frac{1}{4c^2}\hat{L}-\hat{T} \end{bmatrix}U, \\ &= \begin{bmatrix} H_{+}^{X2C1e} & 0 \\ 0 & H_{-}^{X2C1e} \end{bmatrix}. \end{aligned} \tag{1}$$

Here, $\hat{V}$ is the local Coulomb potential, $\hat{T}$ is the kinetic energy matrix, and the $\hat{L}$ operator is defined as

$$\hat{L} = (\vec{\sigma}\cdot\vec{p})\hat{V}(\vec{\sigma}\cdot\vec{p}). \tag{2}$$

The assumption invoked in the X2C formalism is that after the unitary transformation, the large component can be effectively considered as an electron, even though in principle, it mixes the electronic and positronic components. Therefore, the large-component Hamiltonian H_{+}^{X2C1e} is used as the one-body Hamiltonian in electronic structure calculations, along with the usual two-electron integrals. We should note that no relativistic correction is used for the latter.

The formalism described so far is called the X2C1e approximation. By definition, this approximation breaks the S_z spin-symmetry and necessitates the use of generalized spin-orbitals in subsequent calculations. Another approximation, known as the spin-free X2C1e (sfX2C1e) approximation, is also popular. In sfX2C1e, only the spin-independent contribution arising from the $\hat{L}$-operator in eqn (2) is considered. Given that sfX2C1e leads to a symmetry-adapted Hamiltonian, for several systems, where negligible or no SOC is present, using sfX2C1e greatly reduces the computational cost and memory requirements in a calculation, without any accuracy loss. Even when SOC cannot be neglected, total energy trends in sfX2C1e do not differ significantly from X2C1e.[39]

B. Self-consistent *GW*

Hedin's equations[5] define a perturbation theory where the one-particle Green's function G, the vertex function Γ, the irreducible polarizability Π_0, the screened Coulomb interaction W, and the self-energy Σ are related through a set of integro-differential equations. This is traditionally represented as Hedin's pentagram diagram. In the *GW* approximation, higher-order corrections to the vertex arising from G are ignored and the vertex Γ is approximated as a Dirac delta function in space-time. As a result, the self-energy is expressed as a product of the interacting Green's function G and the screened Coulomb potential W.

Hedin's equations or the *GW* approximation can be evaluated either on the real or imaginary axis. Here, we work with the finite-temperature (or Matsubara imaginary axis) formalism described in ref. 63 and 64. The one-particle imaginary-time Green's function is defined as

$$G^{\mathbf{k}}_{p\sigma,q\sigma'}(\tau) = \frac{1}{\mathcal{Z}}\mathrm{Tr}\left(\mathrm{e}^{-(\beta-\tau)(H-\mu N)}c^{\mathbf{k}}_{p\sigma}\mathrm{e}^{-\tau(H-\mu N)}c^{\mathbf{k},\dagger}_{q\sigma'}\right), \tag{3}$$

where Tr denotes trace, $\beta = 1/k_{\mathrm{B}}T$ is the inverse temperature (k_{B} being the Boltzmann constant), μ is the chemical potential, H and N are the Hamiltonian and particle number operators, $c^{\mathbf{k}}_{p\sigma}$ and $c^{\mathbf{k},\dagger}_{p\sigma}$ are the second-quantization annihilation and creation operators for the pth Bloch orbital with the spin σ and momentum label $\mathbf{k}$, and $\tau \in [0, \beta]$ is the imaginary time. Finally, $\mathcal{Z}$ is the partition function, defined as

$$\mathcal{Z} = \mathrm{Tr}\left(\mathrm{e}^{-\beta(H-\mu N)}\right). \tag{4}$$

In the *GW* approximation, the self-energy on the imaginary time/frequency axis is approximated as

$$\boldsymbol{\Sigma}^{\mathbf{k}}[\mathbf{G}](\mathrm{i}\omega_n) = \boldsymbol{\Sigma}^{\mathbf{k}}_{\infty}[\mathbf{G}] + \boldsymbol{\Sigma}^{\mathbf{k}}_{c}[\mathbf{G}](\mathrm{i}\omega_n), \tag{5}$$

where $\boldsymbol{\Sigma}^{\mathbf{k}}_{\infty}$ is the static (frequency-independent) Hartree–Fock self-energy, and $\boldsymbol{\Sigma}^{\mathbf{k}}_{c}(\mathrm{i}\omega_n)$ is the dynamic contribution, defined on the imaginary time (τ) axis as

$$(\boldsymbol{\Sigma}_c)^{\mathbf{k}}_{p\sigma,q\sigma'}(\tau) = -\frac{1}{N_{\mathbf{k}}}\sum_{\mathbf{q}}\sum_{ab} G^{\mathbf{k}-\mathbf{q}}_{a\sigma,b\sigma'}(\tau)\,\tilde{W}^{\mathbf{k}\,\mathbf{k}-\mathbf{q}\,\mathbf{k}-\mathbf{q}\,\mathbf{k}}_{p\,a\quad b\quad q}(-\tau), \tag{6}$$

where $\tilde{W}$ is the effective screened Coulomb interaction, and $N_{\mathbf{k}}$ is the number of k-points sampled in the Brillouin zone (BZ). The summations are performed over momentum vectors $\mathbf{q}$ in the BZ, as well as the atomic orbitals a and b in the unit cell. The new Green's function is then defined by the Dyson equation,

$$[\mathbf{G}^{\mathbf{k}}(\mathrm{i}\omega_n)]^{-1} = (\mathrm{i}\omega_n + \mu)\mathbf{S}^{\mathbf{k}} - \mathbf{H}_0^{\mathbf{k}} - \boldsymbol{\Sigma}^{\mathbf{k}}(\mathrm{i}\omega_n), \tag{7}$$

where the chemical potential μ is fixed to ensure a correct particle number, $\mathbf{S}^{\mathbf{k}}$ is the overlap matrix, and $\mathbf{H}_0^{\mathbf{k}}$ is the one-electron Hamiltonian. We refer the readers to ref. 64 for exact expressions for the screened Coulomb operator $\tilde{W}$. The total electronic energy is calculated using the Galitskii–Migdal formula,

$$E = E_{1\mathrm{b}} + E_{2\mathrm{b}}, \tag{8a}$$

$$E_{1\mathrm{b}} = \frac{1}{2N_{\mathbf{k}}}\sum_{\mathbf{k}}\mathrm{Tr}\left[\boldsymbol{\gamma}^{\mathbf{k}}\left(\mathbf{F}^{\mathbf{k}} + \mathbf{H}_0^{\mathbf{k}}\right)\right], \tag{8b}$$

$$E_{2\mathrm{b}} = \frac{2}{\beta N_{\mathbf{k}}}\sum_{n,\mathbf{k}}\mathrm{Tr}\left[\mathbf{G}^{\mathbf{k}}(\mathrm{i}\omega_n)\boldsymbol{\Sigma}_c^{\mathbf{k}}(\mathrm{i}\omega_n)\right], \tag{8c}$$

where $\mathbf{F}^{\mathbf{k}}$ is the Fock matrix, defined as

$$\mathbf{F}^{\mathbf{k}} = \mathbf{H}_0 + \boldsymbol{\Sigma}_\infty^{\mathbf{k}}, \tag{9}$$

and $\gamma^{\mathbf{k}} = -\mathbf{G}^{\mathbf{k}}(\tau = \beta^-)$ is the one-particle density matrix. In our implementation of sc*GW*, eqn (5)–(7) are solved iteratively until self-consistency is achieved in both the one-body contribution to the energy $E_{1\mathrm{b}}$ as well as the total energy E. Finite-size corrections for the static and dynamic contributions to the self-energy, wherever employed, have been included, as described in ref. 64. Relativistic effects at the level of both spin-free and full X2C formalism with a one-electron approximation (sfX2C1e and X2C1e) have been used.

C. Equation of state for solids

For periodic solids, the relationship between energy and volume in a unit cell is called the equation of state. Several different parametrizations of this equation are available. Fitting the energy-volume data to these forms allows us to estimate the equilibrium volume (and in turn, the lattice constant), the bulk modulus, and other related quantities. One of the most commonly used parametrizations, the Birch–Murnaghan[66] equation of state is defined as

$$E(V) = E_0 + \frac{9B_0V_0}{16}\left\{\left[\left(\frac{V_0}{V}\right)^{2/3} - 1\right]^3 B'_0 + \left[\left(\frac{V_0}{V}\right)^{2/3} - 1\right]^2\left[6 - 4\left(\frac{V_0}{V}\right)^{2/3}\right]\right\}, \tag{10}$$

where E_0, V_0 and B_0 denote the equilibrium energy, volume and bulk modulus, respectively, while B'_0 denotes the derivative of the bulk modulus with respect to the cell volume V, taken at V_0. The Murnaghan[65] and Vinet[82] equations are other

notable parametric forms. For the purpose of this paper, we fit the energy-volume data to eqn (10) using the least-squares optimization.

III. Computational details

All of our calculations are performed with Gaussian-type orbitals (GTO) or their periodic generalizations.[83,84] For initializing all the calculations, we use PySCF[84,85] where we generate the one- and two-electron integrals, and perform mean-field calculations such as Hartree–Fock (HF) or DFT. For the density-fitting in two-electron integrals, we employ even-tempered Gaussian orbitals[86] with progression factor 2.0 for both molecules and extended systems. For the relativistic calculations, we use x2c-nZVPall (n = S, T, Q) family of basis sets.[87] In contrast to the traditionally used uncontracted bases for the relativistic calculations, the x2c family of basis sets contains contracted bases minimizing the number of basis functions without a significant sacrifice of overall accuracy. To construct the initial Dirac Hamiltonian, the basis set is completely uncontracted (as is also programmed, by default, in PySCF).

All the dynamical quantities, *i.e.*, imaginary-time and frequency dependent objects, in sc*GW* are stored using sparse grids.[88–93] Sufficiently large grids are used to avoid loss of information in Fourier transforms performed over successive iterations of the *GW* cycle. To obtain spectral functions, ionization potentials (IPs) and band gaps, the Matsubara Green's function in our calculations is analytically continued to the real-frequency axis. We use the Nevanlinna analytical continuation to accomplish this task.[94] To avoid poles on the real axis, a small broadening, a positive imaginary term, is added to the real-frequency grid, *i.e.*,

$$G(\mathrm{i}\omega_n) \xrightarrow[\text{continuation}]{\text{Nevanlinna analytic}} G(\omega + \mathrm{i}\eta). \tag{11}$$

For IP and band-gap calculations, we employ $\eta = 0.01$ a.u. and $\eta = 0.001$ a.u., respectively. For photoelectron spectra of $HgCl_2$, we have chosen a broadening of $\eta = 0.002$ a.u. to match the experimental peak widths, while in Fig. 1, $\eta = 0.005$ a.u. is used. All our calculations are converged with rigorous thresholds. In particular, we ensure that the particle number is converged to a relative tolerance of 10^{-8} and the total energy to an absolute tolerance of 10^{-5} a.u. The finite-temperature sc*GW* code used here is accessible *via* GitHub.[95]

A. Need for relativistic corrections

Before we begin discussing the challenges associated with the application of relativistic sc*GW*, it is important to justify the necessity of incorporating relativistic effects into correlated all-electron (AE) calculations. We accomplish this by studying the band structure of germanium. In Fig. 1, we plot three different band structure results evaluated using both PBE and sc*GW* for germanium with a diamond lattice, and lattice constant $a = 5.657$ Å. For all these calculations, we used a $6 \times 6 \times 6$ k-mesh sampling in the BZ.

In the top left panel, we employ the GTH basis set and PPs, where the relativistic effects are built directly into the PPs. Here, we find that PBE predicts a semiconducting phase with 0 eV band gap at the Γ point. The top middle and right panels show PBE calculations with and without the inclusion of scalar

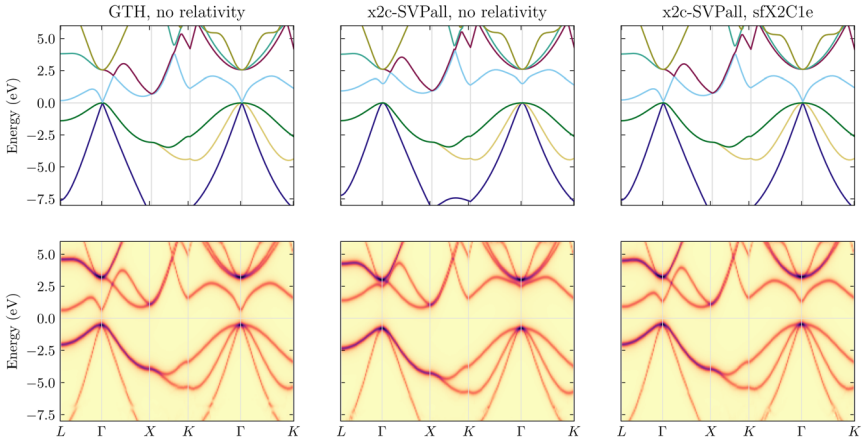

Fig. 1 Band structure of germanium calculated with (top panels) PBE and (lower panels) sc*GW* theories, using the (left) GTH-PBE pseudopotential with GTH-DZVP-MOLOPT-SR basis set, (middle) x2c-SVPall all-electron basis set without relativistic corrections, and (right) x2c-SVPall basis set with sfX2C1e Hamiltonian. For the GTH result, relativity is intrinsically accounted for in the pseudopotential. A diamond lattice with lattice constant $a = 5.657$ Å was used, and all calculations were performed with a $6 \times 6 \times 6$ k-mesh sampling in the BZ.

relativistic effects, respectively. Both were performed using an AE basis, namely x2c-SVPall. Right away, one finds that non-relativistic AE-PBE yields a qualitatively incorrect result with an indirect and sizeable band gap of 1 eV between the Γ and L high-symmetry points. By including scalar relativistic effects at the sfX2C1e level, the band gap is closed resulting in a correct DFT band structure, similar to the GTH results. For germanium, SOC effects are known to be negligible and therefore not considered here.

While both the top left and top right panels of Fig. 1 display the correct band structure of germanium at the PBE level, the experimental results yield a band structure with an indirect band gap of 0.7 eV between the Γ and L points, and this only fortuitously somewhat resembles the band structure from the middle panel evaluated with an AE basis and non-relativistic PBE. Consequently, to recover the experimental result for the right reason, both the relativistic treatment and inclusion of correlation beyond the DFT level is necessary. This is confirmed by the sc*GW* results, shown in the lower panels of Fig. 1. For the sc*GW* results, the band structure for the AE basis set without any relativistic effects is further distorted such that the conduction band, specially near the Γ-point, is pushed upwards and an indirect band gap larger than 2 eV is predicted between the Γ and L points. With appropriate inclusion of relativity, the AE sc*GW* results provide a better quality band structure, with an indirect band gap of ∼1.3 eV, which agrees far better with the experimental value of 0.7 eV.

IV. Results

We are now well-equipped to explore the challenges with relativistic *GW* calculations. In each of the subsections, we describe a specific issue with supporting data. Further analysis and discussion on these results is presented in Section V.

A. Deficiency of pseudopotentials

Modern PPs are designed to account for relativistic effects and, in doing so, eliminate the need for including relativity in subsequent calculations. The GTH PPs and associated basis sets by Goedecker–Teter–Hutter[102,103] constitute one such example. While the use of PPs generally provides a good description of valence-shell band structures, as can be observed from Fig. 1, they are far from adequate for other properties that are generally derivable from total energy. We investigate the performance of AE and PP-based basis sets for three materials with a diamond-lattice: Si, Ge, and αSn. With an increasing atomic number and core size, they serve as excellent representative examples to validate the importance of a proper description of the core orbitals.

In Table 1, by comparing PBE and sc*GW* predictions for lattice constants and bulk moduli against their respective experimental values, we demonstrate that as the atomic number of compounds requiring relativistic treatment increases, and consequently the size of their core (approximated using PPs) increases, the accuracy of the PP-based results decreases, necessitating the use of AE basis sets to achieve agreement with experiments.

For Si, which does not require relativistic corrections, using AE basis set over PPs has virtually no impact on the quality of the results. On the other hand, for αSn, AE results provide a significant improvement, which is even more pronounced in sc*GW* than in PBE. We use the GTH-DZVP-MOLOPT-SR basis set with a GTH-PBE PP for the PP-based calculations, and the x2c-TZVPall basis set, which is the largest basis where we could reliably perform equation-of-state calculations, for AE calculations.

For Si and other elements where the size of the atomic core is small and the relativistic effects are negligible, PPs are usually capable of yielding very good results. However, as the atomic number increases, the problems with PPs become more noticeable, as illustrated for germanium and subsequently α-Sn. In Fig. 2, we showcase more examples where sc*GW* evaluated in AE basis sets provides highly accurate results for both equilibrium lattice constants and bulk moduli. In contrast, the sc*GW* results evaluated using GTH PPs are significantly worse than those obtained with PBE based on GTH PP. Particularly, in ZnX (X = S, Se, Te), AE relativistic sc*GW* is highly effective in contrast to the GTH results. This poor

Table 1 Comparison of the predicted lattice constants and bulk moduli from calculations with AE basis sets against those with PPs. The data highlights the deficiency of PPs in describing energy-derivable bulk properties as atomic number increases resulting in an increase of the PP-approximated core

		Lattice constant (Å)			Bulk modulus (GPa)		
Material	Basis set	PBE	sc*GW*	Exp.	PBE	sc*GW*	Exp.
Si	GTH-DZVP-MOLOPT-SR	5.499	5.456	5.431 (ref. 96)	84.8	96.6	97.9 (ref. 97)
	x2c-TZVPall (sfX2C1e)	5.494	5.413		83.4	102.5	
	def2-TZVP (non-relativistic)	5.491	5.411		84.0	100.9	
Ge	GTH-DZVP-MOLOPT-SR	5.812	5.733	5.657 (ref. 98)	52.8	66.4	75.0 (ref. 99)
	x2c-TZVPall (sfX2C1e)	5.769	5.609		56.9	83.9	
αSn	GTH-DZVP-MOLOPT-SR	6.711	6.649	6.489 (ref. 100)	32.6	32.6	53.1 (ref. 101)
	x2c-TZVPall (sfX2C1e)	6.663	6.391		35.2	54.3	

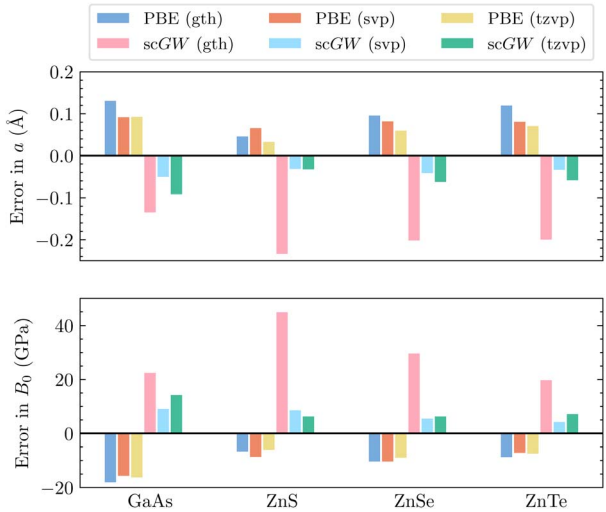

Fig. 2 Errors in (top) lattice constants a, and (bottom) bulk moduli B_0 for selected materials. All compounds are calculated with GTH-DZVP-MOLOPT-SR, x2c-SVPall and x2c-TZVPall basis sets. Both AE-PBE and AE-sc*GW* results are reported using the sfX2C1e Hamiltonian, with a $4 \times 4 \times 4$ k-mesh sampling. Experimental values for lattice constants and bulk moduli can be found in ref. 104, 105 and 106–108 respectively.

performance of GTH PPs with sc*GW* can be attributed to missing correlation contribution arising from the overlap of zinc's inner p and d orbitals with the inner p orbitals of the chalcogen.

In Green's function calculations such as sc*GW*, when AE basis sets are employed, the core orbitals are described by self-energy matrix elements that have both static and dynamic parts. In contrast, when PPs are used, the dynamic part of the self-energy is entirely missing from the description of the core orbitals. For light elements such as Si, the magnitude of the dynamic self-energy for the core orbitals is small, and in addition, there are also only a few core orbitals. Consequently, the error of neglecting these self-energies is overall insignificant. On the other hand, given the large number of core orbitals in heavy elements, the number of dynamic core–core and core–valence self-energy matrix elements neglected by PPs is significant. Moreover, the mixing between valence and outer-core orbitals becomes important, resulting in sizable values of the outer core and core–valence self-energy matrix elements. Since the calculations involving PPs, by design, cannot include any dynamic self-energy for the core, it is reasonable to expect that for elements where such self-energy contributions are significant, the use of PPs will result in sizeable errors. These errors can be additionally compounded by a lack of good, well-optimized PPs for heavier elements. Therefore, it is worth noting that for Green's function methods, the use of PPs poses a different set of problems than for DFT. The DFT results can only be affected by a lack of well-optimized PPs, while Green's function methods would always be penalized by the absence of dynamic self-energy even for the best optimized PPs. For some lighter elements, one can only hope that these dynamic self-energy matrix elements have insignificant values; however, this assumption cannot be generally fulfilled.

Table 2 PBE0 and sc*GW* results for ionization potentials (in eV) for selected silver halides. The results were evaluated using different basis sets and then extrapolated to the basis-set limit. Notice that the mean-field method appears to be converged already at the triple-ζ level

	AgCl		AgBr		AgI	
Basis	PBE0	sc*GW*	PBE0	sc*GW*	PBE0	sc*GW*
x2c-TZVPall	7.51	9.54	7.18	9.11	6.77	8.46
x2c-QZVPall	7.58	9.78	7.23	9.29	6.83	8.64
Extrapolated	7.67	10.09	7.29	9.53	6.89	8.86

B. Convergence issues in basis sets

For heavy elements, the very large size of the one-electron basis sets effectively hinders the ability to investigate convergence with respect to basis-set size in AE calculations. While for molecules, this formidable challenge can still be overcome, it becomes insurmountable in calculations of solids. The problem is relatively mild, often almost non-existent, at the level of DFT or HF, but quickly becomes aggravated for correlated calculations such as sc*GW*. This can also be understood by the fact that basis sets are usually optimized at the atomic level using SCF calculations. Such behavior has also been observed by Kutepov in ref. 44, where DFT calculations converged far more rapidly than sc*GW* while using linearized augmented-plane-wave (LAPW) basis functions. Here, we examine such convergence issues in detail.

First, we look at IPs for AgCl, AgBr and AgI, which are representative examples of closed-shell relativistic molecules with increasing SOC as we go from Cl to I. These systems have been widely used to benchmark recent implementations of relativistic *GW* methods.[37,39,60] For these molecules, in Table 2, we show IPs evaluated in PBE0 and sc*GW* with x2c-TZVPall and x2c-QZVPall basis sets. Using these two IP values, an extrapolated IP value (also reported in Table 2) is calculated assuming an inverse relationship between IP and the number of atomic orbitals (AOs) in the respective basis set. We use the scalar relativistic Hamiltonian in all these calculations. Comparing these trends graphically in Fig. 3, we can

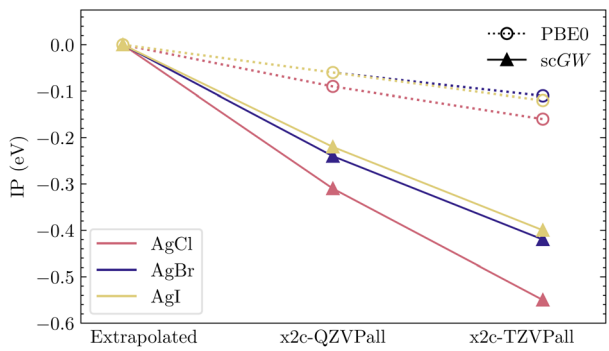

Fig. 3 Graphical representation of convergence trends in Table 2. All IPs are reported relative to the respective extrapolated values, which shows that sc*GW* exhibits a much slower convergence than PBE0.

Table 3 Convergence of PBE and sc*GW* band gaps for AgBr and CdSe, with respect to basis sets from the x2c family. The results were calculated with the sfX2C1e-Coulomb Hamiltonian and a $4 \times 4 \times 4$ k-mesh and inverse temperature $\beta = 300$ a.u.$^{-1}$ (for sc*GW*). The total numbers of GTOs per cell for each basis set are listed in the second column

		L–L		Γ–Γ		X–X		L–Γ	
Basis	Orbitals	PBE	sc*GW*	PBE	sc*GW*	PBE	sc*GW*	PBE	sc*GW*
AgBr									
x2c-SVPall	85	3.887	6.73	2.536	5.38	3.926	7.68	0.699	3.71
x2c-TZVPall	111	3.833	6.50	2.529	5.23	3.901	7.49	0.688	3.54
x2c-QZVPall	167	3.776	6.31	2.546	5.00	3.886	7.17	0.678	3.34
CdSe									
x2c-SVPall	88	3.209	5.53	0.663	2.73	5.006	6.98	1.428	3.60
x2c-TZVPall	111	3.193	5.46	0.659	2.69	5.004	6.94	1.433	3.55
x2c-QZVPall	192	3.179	5.30	0.633	2.56	5.003	6.87	1.406	3.40

clearly observe that for PBE0, the extrapolated IPs are within 0.1 eV of QZ, displaying a fast convergence. However, for sc*GW*, the quadruple-ζ results are far from converged, with extrapolation leading to changes of more than 0.2 eV. It is worth mentioning that an extrapolation based on two calculations, triple- and quadruple-ζ, is already far from ideal, especially when the resultant corrections are so large. Having quintuple-ζ results would greatly enhance the quality of the results. However, even without considering the computational challenge that such a calculation poses, in many relativistic basis sets, including x2c, quintuple-ζ bases are simply not available.

Next, we look at the band structure in relativistic solids, with a focus on AgBr and CdSe. For AgBr, a rock-salt crystal structure with $a = 5.774$ Å is considered, while the zinc blende phase in CdSe with $a = 6.05$ Å is used. All calculations were performed using a $4 \times 4 \times 4$ k-mesh sampling, using x2c-SVPall, x2c-TZVPall and x2c-QZVPall basis sets. An inverse temperature of $\beta = 300$ a.u.$^{-1}$ was used. For the QZVPall basis with AgBr, diffuse s and p orbitals with Gaussian exponents smaller than 0.05 were removed to avoid linear dependencies in the basis set. High angular momentum g-orbitals were removed from the QZVPall basis set in both systems.

For AgBr, in ref. 63, Yeh *et al.* noted poor convergence of band-gap values along the path containing special symmetry points. Here we present further data contrasting sc*GW* convergence trends against PBE.

In Table 3, we present direct and indirect band gaps in AgBr and CdSe, with x2c-SVPall, x2c-TZVPall and x2c-QZVPall basis sets. Already at the triple-ζ level, for both systems, PBE band gaps are well converged to within 0.05 eV when compared with the quadruple-ζ basis. However, sc*GW* once again shows much slower convergence trends, and going from triple- to quadruple-ζ still introduces corrections larger than 0.1 eV for CdSe and 0.2 eV for AgBr.

Finally, in Table 4 we show convergence trends for lattice constants of Si, Ge, GaAs, αSn, and InSb. All these systems have a diamond (zinc blende for GaAs and InSb) structure, with an increasing size of atomic core as we go from Si to InSb. Similar to previous observations, the convergence of sc*GW* values is more than 2–

Table 4 Basis set convergence trends in lattice constants [Å] for selected compounds. Results for x2c-SVPall and x2c-TZVPall basis sets are shown, denoted by SVP and TZVP, respectively. For readers' convenience, we also list the difference between them

	PBE			sc*GW*			
System	SVP	TZVP	Diff.	SVP	TZVP	Diff.	Exp.
Si	5.504	5.494	−0.010	5.453	5.413	−0.04	5.431 (ref. 96)
Ge	5.779	5.773	−0.006	5.622	5.559	−0.063	5.657 (ref. 98)
GaAs	5.747	5.748	0.001	5.600	5.559	−0.041	5.653 (ref. 104)
α-Sn	6.620	6.663	0.043	6.456	6.391	−0.065	6.489 (ref. 100)
InSb	6.597	6.64	0.043	6.463	6.381	−0.082	6.479 (ref. 109)

3 times slower than for PBE. At the level of DFT, it seems that only for Si does the larger basis set marginally improve the agreement with experiment, while for all the other materials, the results either do not change or become worse. Consequently, one can suspect that DFT optimization of higher level bases is not as effective as lower level bases since the convergence with respect to the basis size is achieved relatively early on. This suspicion is somewhat confirmed when examining the sc*GW* results. Almost all SVPall sc*GW* results are surprisingly close to experiment and do not seem to be improved in a larger basis. For periodic systems, an extrapolation procedure, similar to the one used for molecular IPs, cannot be considered. This is because SVP is not a sufficiently large basis and using it together with only the TZVP basis would lead to largely inaccurate extrapolated data. While for molecular systems, QZ-level calculations remain accessible and make extrapolations possible, for the periodic systems, these calculations are extremely expensive and mostly out of reach.

C. Linear dependencies

For correlated calculations, the quest for converging properties to a complete basis-set limit is not only affected by slower convergence and a lack of larger basis sets, but also by linear dependencies arising in the large basis sets. Particularly in solids, due to close packing of atoms, adding more basis functions introduces strong linear dependencies among the atomic orbitals. As a result, the condition number of the overlap matrix becomes too large even for an easy execution of mean-field methods. The problem of linear dependencies is not unique to the GTOs considered here, and has been reported in other kinds of orbital representations, namely Slater-type orbitals (STO), and also in LAPW.[36,110–112]

Even though linear dependencies are more severe in ionic compounds, they also remain problematic in covalent compounds (such as silicon) and arise at small bond distances in all compounds. One way to remedy this problem in GTO basis sets is to simply remove the diffuse functions. These orbitals have long tails because of their small Gaussian exponents, leading to an increased overlap with other atomic orbitals. However, when studying bulk properties, such a procedure generally does more harm than good. When the bonds are stretched, the lack of diffuse orbitals leads to a deficient description of atomic bonds and substantially alters the equation of state, causing significant errors in both the equilibrium lattice constant and bulk modulus. This phenomenon is investigated for silicon

Table 5 Lattice constants a and bulk modulus B_0 for silicon, calculated using the def2-TZVP basis with and without diffuse orbitals (Gaussian exponent < 0.1). Both PBE and sc*GW* results, along with experimental values, are shown. A non-relativistic Hamiltonian was employed for these calculations

Method	a (Å)	B_0 (GPa)
PBE	5.491	84.01
PBE w/o diffuse orbs.	5.378	124.04
sc*GW*	5.411	100.93
sc*GW* w/o diffuse orbs.	5.306	146.88
Experiment[96,97]	5.431	97.8

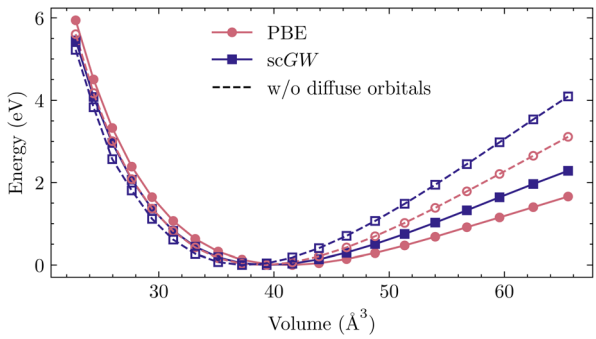

Fig. 4 Energy–volume curves corresponding to Table 5.

in Table 5 and Fig. 4, where we have considered a rather simple case of non-relativistic calculation involving the widely used def2-TZVP basis set. Here, all orbitals with Gaussian exponents smaller than 0.1 were dropped, leading to lattice constants differing by more than 0.1 Å and over 50% error in the bulk modulus. Note that an ad-hoc re-introduction of diffuse functions as we stretch the bonds introduces jumps in the energy–volume curve, precluding a reliable fit to the Birch–Murnaghan equation. Even though the computational cost is still affordable, due to arising linear dependencies, converging DFT and *GW* calculations for Si with a larger basis set proves extremely challenging and is therefore not pursued here.

D. Lack of an accurate experimental reference

To benchmark new theoretical methods that are pushing the limits of accuracy and applicability, reliable experimental references are necessary. Here, we consider the $HgCl_2$ molecule as an example to highlight a potential area where better experimental data can provide feedback to improve theoretical methods. In Fig. 5, we compare sc*GW* results with two different experimental spectra for $HgCl_2$. In one of the experiments by Boggess *et al.*[113] (labeled Exp-1 in the plot), the SOC splitting is unresolved in both the first and second IPs. Results by Eland *et al.*[114] (Exp-2 in Fig. 5) clearly resolve the SOC splitting in the first IP ($^2\Pi_g$ state), but report difficulty with the second peak ($^2\Pi_u$ state). Among the *GW* results, scalar relativistic corrections (sfX2C1e) capture the overall peak structure,

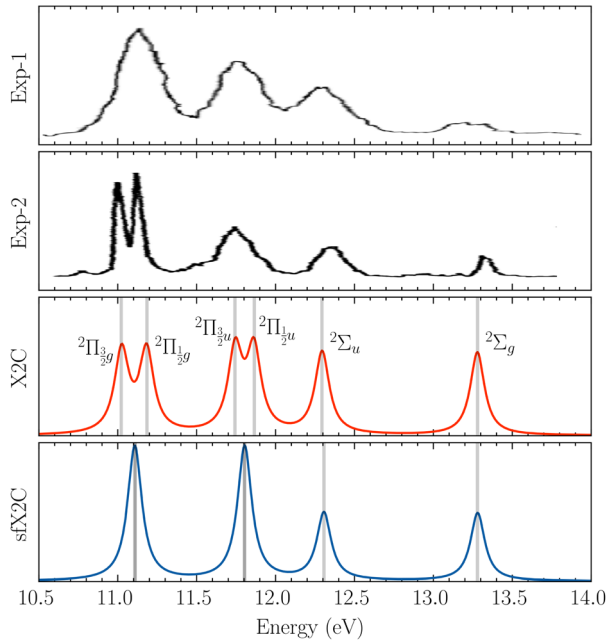

Fig. 5 Comparison of experimental spectra with sc*GW* results for $HgCl_2$, obtained with both scalar and two-component relativistic effects. For these calculations, we have used the x2c-QZVPall basis. Both experimental spectra, Exp-1 by Boggess *et al.*[113] and Exp-2 by Eland *et al.*,[114] are shifted by 0.35 eV to match the associated IP peaks.

producing a spectra similar to Exp-1. However, the spin-free theory understandably misses out on the SOC splitting, which, in turn, is captured at the X2C1e level. In fact, for sc*GW* with X2C1e, spin–orbit splitting is visible for both $^2\Pi_g$ and $^2\Pi_u$ states. For the first ionization peak, sc*GW* predicts a 0.16 eV splitting for the $^2\Pi_{\frac{3}{2}g}$ and $^2\Pi_{\frac{1}{2}g}$ states, which is close to the experimental value of 0.12 eV. Similarly, for the $^2\Pi_{\frac{3}{2}u}$ and $^2\Pi_{\frac{1}{2}u}$ states, a splitting of 0.12 eV is predicted, but the corresponding results are not resolved in the experiments.

V. Discussion and conclusions

We have presented ample numerical evidence that when employing Green's function methods, particularly sc*GW*, the current frameworks of PPs and orbital representation encounter challenges in fully realizing the potential of precise quantum chemistry calculations for relativistic systems. One of the challenges is that PPs are not adept in accurately describing properties other than valence-shell electronic structure, such as band gaps and ionization potentials. When a material is pressurized, *e.g.*, while studying the equation of state, the correlation effects arising from the overlap between atomic cores cannot be captured by PPs, and highly expensive AE calculations become unavoidable. Effective cores and PPs where a smaller number of electrons are modelled as part of the core offer one way

to overcome this hurdle, and while some candidates are available,[115–119] more developments and systematic benchmarks of new ECPs and PPs are desirable.

Additionally, it should be noted that when using PPs in Green's function methods, there is an inherent error that comes from the absence of dynamic self-energy matrix elements for core and core–valence sectors, even if the best optimized PPs are employed. Especially for heavier elements, one can surmise that such a PP approximation will lead to significant errors since both the values and the number of outer-core dynamic self-energy matrix elements may be large. Consequently, even with the most optimized PPs, as they are formulated now, we can expect significant errors.

For correlated methods such as sc*GW*, understanding the basis set convergence is a bit difficult. Even when well designed and optimized basis sets are available,[120] correlated methods generally exhibit a slower convergence than mean-field ones. Yet, the fact that basis sets are optimized at the level of mean-field cannot be overlooked and, in fact, is potentially one of the reasons behind faster convergence in DFT and HF.[121,122] For lighter elements, basis-set convergence is easily achieved and such problems do not require any particular attention. However, the same is not true for heavy elements where relativity is also important. The issues with basis sets for heavy elements is well known and has been a topic of recent research.[123,124]

Furthermore, most quantum chemistry basis sets have been optimized for molecular applications. When these are applied to solids, not only may the molecular level optimization prove insufficient, additional problems related to linear dependency and unfavorable convergence trends are more prone to arise. Recently, Ye *et al.*[125] also noticed similar problems and proposed correlation-consistent basis sets optimized for solids. Another way to improve the quality of basis sets is to perform a material-specific optimization.[126] These developments, including other means to eliminate linear dependencies,[127,128] are yet to be applied to relativistic materials and molecules. It is also likely that a better one-particle orbital representation, with strictly orthogonal atomic orbitals, may be required to simultaneously overcome the issues related to convergence and linear-dependencies.[129–131] Consequently, one can expect that in the future explicitly orthogonal single-particle orbitals, such as tensor-train numerical STOs,[132] or orthogonal gausslets,[129–131] will show promise to solve the problem of linear dependency. Constructing PPs and basis functions from correlated calculations may also offer a viable route to improve the reliability of relativistic calculations.

Lastly, we also show that as theoretical methods become more accurate, better and reliable experimental benchmarking data with well-resolved photoelectron spectra are desirable to both validate theoretical results and push for new theoretical developments.

Conflicts of interest

There are no conflicts to declare.

Acknowledgements

This material is based upon work supported by the U.S. Department of Energy, Office of Science, Office of Advanced Scientific Computing Research and Office of

Basic Energy Sciences, Scientific Discovery through Advanced Computing (SciDAC) program under Award Number DE-SC0022198. This research used resources of the National Energy Research Scientific Computing Center, a DOE Office of Science User Facility supported by the Office of Science of the U.S. Department of Energy under Contract No. DE-AC02-05CH11231 using NERSC awards BES-ERCAP0029462 and BES-ERCAP0024293.

References

1 W. Kohn and J. M. Luttinger, Ground-State Energy of a Many-Fermion System, *Phys. Rev.*, 1960, **118**, 41.
2 W. Kohn and L. J. Sham, Self-Consistent Equations Including Exchange and Correlation Effects, *Phys. Rev.*, 1965, **140**, A1133.
3 T. D. Crawford and H. F. Schaefer, An Introduction to Coupled Cluster Theory for Computational Chemists, in *Reviews in Computational Chemistry*, ed. K. B. Lipkowitz and D. B. Boyd, John Wiley & Sons, Inc., 2000, pp. 33–136.
4 R. J. Bartlett and M. Musiał, Coupled-cluster theory in quantum chemistry, *Rev. Mod. Phys.*, 2007, **79**, 291.
5 L. Hedin, New Method for Calculating the One-Particle Green's Function with Application to the Electron-Gas Problem, *Phys. Rev.*, 1965, **139**, A796.
6 N. E. Dahlen and R. van Leeuwen, Self-consistent solution of the Dyson equation for atoms and molecules within a conserving approximation, *J. Chem. Phys.*, 2005, **122**, 164102.
7 J. J. Phillips and D. Zgid, Communication: the description of strong correlation within self-consistent Green's function second-order perturbation theory, *J. Chem. Phys.*, 2014, **140**, 241101.
8 A. A. Rusakov and D. Zgid, Self-consistent second-order Green's function perturbation theory for periodic systems, *J. Chem. Phys.*, 2016, **144**, 054106.
9 G. P. Chen, V. K. Voora, M. M. Agee, S. G. Balasubramani and F. Furche, Random-Phase Approximation Methods, *Annu. Rev. Phys. Chem.*, 2017, **68**, 421.
10 A. Georges, G. Kotliar, W. Krauth and M. J. Rozenberg, Dynamical mean-field theory of strongly correlated fermion systems and the limit of infinite dimensions, *Rev. Mod. Phys.*, 1996, **68**, 13.
11 A. I. Lichtenstein, M. I. Katsnelson and G. Kotliar, Finite-Temperature Magnetism of Transition Metals: An ab initio Dynamical Mean-Field Theory, *Phys. Rev. Lett.*, 2001, **87**, 067205.
12 G. Kotliar, S. Y. Savrasov, K. Haule, V. S. Oudovenko, O. Parcollet and C. A. Marianetti, Electronic structure calculations with dynamical mean-field theory, *Rev. Mod. Phys.*, 2006, **78**, 865.
13 G. Knizia and G. K.-L. Chan, Density Matrix Embedding: A Simple Alternative to Dynamical Mean-Field Theory, *Phys. Rev. Lett.*, 2012, **109**, 186404.
14 A. A. Kananenka, E. Gull and D. Zgid, Systematically improvable multiscale solver for correlated electron systems, *Phys. Rev. B: Condens. Matter Mater. Phys.*, 2015, **91**, 121111.
15 T. N. Lan, A. A. Kananenka and D. Zgid, Communication: towards ab initio self-energy embedding theory in quantum chemistry, *J. Chem. Phys.*, 2015, **143**, 241102.

16 S. Wouters, C. A. Jiménez-Hoyos, Q. Sun and G. K.-L. Chan, A Practical Guide to Density Matrix Embedding Theory in Quantum Chemistry, *J. Chem. Theory Comput.*, 2016, **12**, 2706.
17 D. Zgid and E. Gull, Finite temperature quantum embedding theories for correlated systems, *New J. Phys.*, 2017, **19**, 023047.
18 A. A. Rusakov, S. Iskakov, L. N. Tran and D. Zgid, Self-Energy Embedding Theory (SEET) for Periodic Systems, *J. Chem. Theory Comput.*, 2019, **15**, 229.
19 C. Sun, U. Ray, Z.-H. Cui, M. Stoudenmire, M. Ferrero and G. K.-L. Chan, Finite-temperature density matrix embedding theory, *Phys. Rev. B*, 2020, **101**, 075131.
20 F. Aryasetiawan and O. Gunnarsson, TheGW method, *Rep. Prog. Phys.*, 1998, **61**, 237.
21 D. Golze, M. Dvorak and P. Rinke, The GW Compendium: A Practical Guide to Theoretical Photoemission Spectroscopy, *Front. Chem.*, 2019, **7**, 377.
22 L. Reining, The GW approximation: content, successes and limitations, *Wiley Interdiscip. Rev.: Comput. Mol. Sci.*, 2018, **8**, e1344.
23 O. Vahtras, J. Almlöf and M. W. Feyereisen, Integral approximations for LCAO-SCF calculations, *Chem. Phys. Lett.*, 1993, **213**, 514.
24 Q. Sun, T. C. Berkelbach, J. D. McClain and G. K.-L. Chan, Gaussian and plane-wave mixed density fitting for periodic systems, *J. Chem. Phys.*, 2017, **147**, 164119.
25 H.-Z. Ye and T. C. Berkelbach, Fast periodic Gaussian density fitting by range separation, *J. Chem. Phys.*, 2021, **154**, 131104.
26 G. E. Scuseria, T. M. Henderson and I. W. Bulik, Particle-particle and quasiparticle random phase approximations: connections to coupled cluster theory, *J. Chem. Phys.*, 2013, **139**, 104113.
27 M. F. Lange and T. C. Berkelbach, On the Relation between Equation-of-Motion Coupled-Cluster Theory and the GW Approximation, *J. Chem. Theory Comput.*, 2018, **14**, 4224.
28 R. Quintero-Monsebaiz, E. Monino, A. Marie and P.-F. Loos, Connections between many-body perturbation and coupled-cluster theories, *J. Chem. Phys.*, 2022, **157**, 231102.
29 J. Tölle and G. Kin-Lic Chan, Exact relationships between the GW approximation and equation-of-motion coupled-cluster theories through the quasi-boson formalism, *J. Chem. Phys.*, 2023, **158**, 124123.
30 A. Stan, N. E. Dahlen and R. v. Leeuwen, Fully self-consistent GW calculations for atoms and molecules, *Europhys. Lett.*, 2006, **76**, 298.
31 F. Caruso, P. Rinke, X. Ren, M. Scheffler and A. Rubio, Unified description of ground and excited states of finite systems: the self-consistent *GW* approach, *Phys. Rev. B: Condens. Matter Mater. Phys.*, 2012, **86**, 081102.
32 N. Marom, F. Caruso, X. Ren, O. T. Hofmann, T. Körzdörfer, J. R. Chelikowsky, A. Rubio, M. Scheffler and P. Rinke, Benchmark of *GW* methods for azabenzenes, *Phys. Rev. B: Condens. Matter Mater. Phys.*, 2012, **86**, 245127.
33 M. J. van Setten, F. Weigend and F. Evers, The GW-Method for Quantum Chemistry Applications: Theory and Implementation, *J. Chem. Theory Comput.*, 2013, **9**, 232.
34 M. J. van Setten, F. Caruso, S. Sharifzadeh, X. Ren, M. Scheffler, F. Liu, J. Lischner, L. Lin, J. R. Deslippe, S. G. Louie, C. Yang, F. Weigend,

J. B. Neaton, F. Evers and P. Rinke, GW100: Benchmarking G0W0 for Molecular Systems, *J. Chem. Theory Comput.*, 2015, **11**, 5665.
35 F. Caruso, M. Dauth, M. J. van Setten and P. Rinke, Benchmark of GW Approaches for the GW100 Test Set, *J. Chem. Theory Comput.*, 2016, **12**, 5076.
36 A. Förster and L. Visscher, Low-Order Scaling Quasiparticle Self-Consistent GW for Molecules, *Front. Chem.*, 2021, **9**, 736591.
37 A. Förster, E. van Lenthe, E. Spadetto and L. Visscher, Two-Component GW Calculations: Cubic Scaling Implementation and Comparison of Vertex-Corrected and Partially Self-Consistent GW Variants, *J. Chem. Theory Comput.*, 2023, **19**, 5958.
38 M. Wen, V. Abraham, G. Harsha, A. Shee, B. Whaley and D. Zgid, Comparing self-consistent GW and vertex corrected G0W0 (G0W0Γ) accuracy for molecular ionization potentials, *arXiv*, 2023, arXiv:2311.12209 [physics:chem-ph], DOI: **10.48550/arXiv.2311.12209**.
39 V. Abraham, G. Harsha and D. Zgid, Relativistic fully self-consistent GW for molecules: total energies and ionization potentials, *arXiv*, 2024, arXiv:2401.11303 [physics:chem-ph], DOI: **10.48550/arXiv.2401.11303**.
40 S. V. Faleev, M. van Schilfgaarde and T. Kotani, All-Electron Self-Consistent *GW* Approximation: Application to Si, MnO, and NiO, *Phys.Rev. Lett.*, 2004, **93**, 126406.
41 M. Shishkin and G. Kresse, Self-consistent *GW* calculations for semiconductors and insulators, *Phys. Rev. B: Condens. Matter Mater. Phys.*, 2007, **75**, 235102.
42 A. Kutepov, S. Y. Savrasov and G. Kotliar, Ground-state properties of simple elements from GW calculations, *Phys. Rev. B: Condens. Matter Mater. Phys.*, 2009, **80**, 041103.
43 A. L. Kutepov, Self-consistent solution of Hedin's equations: semiconductors and insulators, *Phys. Rev. B*, 2017, **95**, 195120.
44 A. L. Kutepov, Ground state properties of 3d metals from self-consistent GW approach, *J. Phys.: Condens. Matter*, 2017, **29**, 465503.
45 M. Grumet, P. Liu, M. Kaltak, J. Klimeš and G. Kresse, Beyond the quasiparticle approximation: fully self-consistent *GW* calculations, *Phys. Rev. B*, 2018, **98**, 155143.
46 P. Pyykkö, Relativistic Effects in Chemistry: More Common Than You Thought, *Annu. Rev. Phys. Chem.*, 2012, **63**, 45.
47 G. Breit, Dirac's Equation and the Spin-Spin Interactions of Two Electrons, *Phys. Rev.*, 1932, **39**, 616.
48 M. Douglas and N. M. Kroll, Quantum electrodynamical corrections to the fine structure of helium, *Ann. Phys.*, 1974, **82**, 89.
49 B. A. Hess, Applicability of the no-pair equation with free-particle projection operators to atomic and molecular structure calculations, *Phys. Rev. A*, 1985, **32**, 756.
50 B. A. Hess, Relativistic electronic-structure calculations employing a two-component no-pair formalism with external-field projection operators, *Phys. Rev. A*, 1986, **33**, 3742.
51 T. Nakajima and K. Hirao, The Douglas–Kroll–Hess Approach, *Chem. Rev.*, 2012, **112**, 385.
52 M. Reiher and A. Wolf, Douglas–Kroll–Hess Theory, in *Relativistic Quantum Chemistry*, John Wiley & Sons, Ltd, 2014, pp. 469–501.

53 W. Kutzelnigg and W. Liu, Quasirelativistic theory equivalent to fully relativistic theory, *J. Chem. Phys.*, 2005, **123**, 241102.
54 W. Liu and W. Kutzelnigg, Quasirelativistic theory. II. Theory at matrix level, *J. Chem. Phys.*, 2007, **126**, 114107.
55 W. Liu and D. Peng, Exact two-component Hamiltonians revisited, *J. Chem. Phys.*, 2009, **131**, 031104.
56 Q. Sun, W. Liu, Y. Xiao and L. Cheng, Exact two-component relativistic theory for nuclear magnetic resonance parameters, *J. Chem. Phys.*, 2009, **131**, 081101.
57 L. Cheng and J. Gauss, Analytic energy gradients for the spin-free exact two-component theory using an exact block diagonalization for the one-electron Dirac Hamiltonian, *J. Chem. Phys.*, 2011, **135**, 084114.
58 R. Sakuma, C. Friedrich, T. Miyake, S. Blügel and F. Aryasetiawan, *GW* calculations including spin-orbit coupling: application to Hg chalcogenides, *Phys. Rev. B: Condens. Matter Mater. Phys.*, 2011, **84**, 085144.
59 A. Kutepov, K. Haule, S. Y. Savrasov and G. Kotliar, Electronic structure of Pu and Am metals by self-consistent relativistic *GW* method, *Phys. Rev. B: Condens. Matter Mater. Phys.*, 2012, **85**, 155129.
60 P. Scherpelz, M. Govoni, I. Hamada and G. Galli, Implementation and Validation of Fully Relativistic GW Calculations: Spin–Orbit Coupling in Molecules, Nanocrystals, and Solids, *J. Chem. Theory Comput.*, 2016, **12**, 3523.
61 C. Holzer and W. Klopper, Ionized, electron-attached, and excited states of molecular systems with spin–orbit coupling: two-component GW and Bethe–Salpeter implementations, *J. Chem. Phys.*, 2019, **150**, 204116.
62 M. Kühn and F. Weigend, One-Electron Energies from the Two-Component GW Method, *J. Chem. Theory Comput.*, 2015, **11**, 969.
63 C.-N. Yeh, A. Shee, Q. Sun, E. Gull and D. Zgid, Relativistic self-consistent *GW*: exact two-component formalism with one-electron approximation for solids, *Phys. Rev. B*, 2022, **106**, 085121.
64 C.-N. Yeh, S. Iskakov, D. Zgid and E. Gull, Fully self-consistent finite-temperature *GW* in Gaussian Bloch orbitals for solids, *Phys. Rev. B*, 2022, **106**, 235104.
65 F. D. Murnaghan, The Compressibility of Media under Extreme Pressures, *Proc. Natl. Acad. Sci. U. S. A.*, 1944, **30**, 244.
66 F. Birch, Finite Elastic Strain of Cubic Crystals, *Phys. Rev.*, 1947, **71**, 809.
67 M. van Schilfgaarde, T. Kotani and S. Faleev, Quasiparticle Self-Consistent *GW* Theory, *Phys. Rev. Lett.*, 2006, **96**, 226402.
68 T. Kotani, M. van Schilfgaarde and S. V. Faleev, Quasiparticle self-consistent *GW* method: a basis for the independent-particle approximation, *Phys. Rev. B: Condens. Matter Mater. Phys.*, 2007, **76**, 165106.
69 H. Cao, Z. Yu, P. Lu and L.-W. Wang, Fully converged plane-wave-based self-consistent *GW* calculations of periodic solids, *Phys. Rev. B*, 2017, **95**, 035139.
70 S. V. Faleev, M. van Schilfgaarde and T. Kotani, All-electron self-consistent *GW* approximation: application to Si, MnO, and NiO, *Phys. Rev. Lett.*, 2004, **93**, 126406.
71 M. van Schilfgaarde, T. Kotani and S. Faleev, Quasiparticle self-consistent *GW* theory, *Phys. Rev. Lett.*, 2006, **96**, 226402.
72 T. A. Pham, H.-V. Nguyen, D. Rocca and G. Galli, *GW* calculations using the spectral decomposition of the dielectric matrix: verification, validation, and

comparison of methods, *Phys. Rev. B: Condens. Matter Mater. Phys.*, 2013, **87**, 155148.

73 M. Govoni and G. Galli, Large scale GW calculations, *J. Chem. Theory Comput.*, 2015, **11**, 2680.

74 S. Biermann, F. Aryasetiawan and A. Georges, First-principles approach to the electronic structure of strongly correlated systems: combining the *GW* approximation and dynamical mean-field theory, *Phys. Rev. Lett.*, 2003, **90**, 086402.

75 F. Nilsson, L. Boehnke, P. Werner and F. Aryasetiawan, Multitier self-consistent *GW* + EDMFT, *Phys. Rev. Mater.*, 2017, **1**, 043803.

76 S. Choi, A. Kutepov, K. Haule, M. van Schilfgaarde and G. Kotliar, First-principles treatment of Mott insulators: linearized QSGW+DMFT approach, *npj Quantum Mater.*, 2016, **1**, 16001.

77 T. N. Lan, A. Shee, J. Li, E. Gull and D. Zgid, Testing self-energy embedding theory in combination with GW, *Phys. Rev. B*, 2017, **96**, 155106.

78 T. Zhu and G. K.-L. Chan, Ab initio full cell *GW* + DMFT for correlated materials, *Phys. Rev. X*, 2021, **11**, 021006.

79 S. Iskakov, C.-N. Yeh, E. Gull and D. Zgid, Ab initio self-energy embedding for the photoemission spectra of NiO and MnO, *Phys. Rev. B*, 2020, **102**, 085105.

80 C.-N. Yeh, S. Iskakov, D. Zgid and E. Gull, Electron correlations in the cubic paramagnetic perovskite Sr(V, Mn)o_3: results from fully self-consistent self-energy embedding calculations, *Phys. Rev. B*, 2021, **103**, 195149.

81 J. Liu, Y. Shen, A. Asthana and L. Cheng, Two-component relativistic coupled-cluster methods using mean-field spin-orbit integrals, *J. Chem. Phys.*, 2018, **148**, 034106.

82 P. Vinet, J. R. Smith, J. Ferrante and J. H. Rose, Temperature effects on the universal equation of state of solids, *Phys. Rev. B: Condens. Matter Mater. Phys.*, 1987, **35**, 1945.

83 R. Dovesi, R. Orlando, C. Roetti, C. Pisani and V. Saunders, The Periodic Hartree-Fock Method and Its Implementation in the Crystal Code, *Phys. Status Solidi B*, 2000, **217**, 63.

84 Q. Sun, X. Zhang, S. Banerjee, P. Bao, M. Barbry, N. S. Blunt, N. A. Bogdanov, G. H. Booth, J. Chen, Z.-H. Cui, J. J. Eriksen, Y. Gao, S. Guo, J. Hermann, M. R. Hermes, K. Koh, P. Koval, S. Lehtola, Z. Li, J. Liu, N. Mardirossian, J. D. McClain, M. Motta, B. Mussard, H. Q. Pham, A. Pulkin, W. Purwanto, P. J. Robinson, E. Ronca, E. R. Sayfutyarova, M. Scheurer, H. F. Schurkus, J. E. T. Smith, C. Sun, S.-N. Sun, S. Upadhyay, L. K. Wagner, X. Wang, A. White, J. D. Whitfield, M. J. Williamson, S. Wouters, J. Yang, J. M. Yu, T. Zhu, T. C. Berkelbach, S. Sharma, A. Y. Sokolov and G. K.-L. Chan, Recent developments in the PySCF program package, *J. Chem. Phys.*, 2020, **153**, 024109.

85 Q. Sun, T. C. Berkelbach, N. S. Blunt, G. H. Booth, S. Guo, Z. Li, J. Liu, J. D. McClain, E. R. Sayfutyarova, S. Sharma, S. Wouters and G. K.-L. Chan, PySCF: the Python-based simulations of chemistry framework, *Wiley Interdiscip. Rev.: Comput. Mol. Sci.*, 2018, **8**, e1340.

86 G. L. Stoychev, A. A. Auer and F. Neese, Automatic Generation of Auxiliary Basis Sets, *J. Chem. Theory Comput.*, 2017, **13**, 554.

87 P. Pollak and F. Weigend, Segmented contracted error-consistent basis sets of double- and triple-ζ valence quality for one- and two-component relativistic all-electron calculations, *J. Chem. Theory Comput.*, 2017, **13**, 3696.
88 A. A. Kananenka, J. J. Phillips and D. Zgid, Efficient temperature-dependent green's functions methods for realistic systems: compact grids for orthogonal polynomial transforms, *J. Chem. Theory Comput.*, 2016, **12**, 564.
89 A. A. Kananenka, A. R. Welden, T. N. Lan, E. Gull and D. Zgid, Efficient temperature-dependent green's function methods for realistic systems: using cubic spline interpolation to approximate Matsubara Green's functions, *J. Chem. Theory Comput.*, 2016, **12**, 2250.
90 E. Gull, S. Iskakov, I. Krivenko, A. A. Rusakov and D. Zgid, Chebyshev polynomial representation of imaginary-time response functions, *Phys. Rev. B*, 2018, **98**, 075127.
91 X. Dong, D. Zgid, E. Gull and H. U. R. Strand, Legendre-spectral Dyson equation solver with super-exponential convergence, *J. Chem. Phys.*, 2020, **152**, 134107.
92 J. Li, M. Wallerberger, N. Chikano, C.-N. Yeh, E. Gull and H. Shinaoka, Sparse sampling approach to efficient ab initio calculations at finite temperature, *Phys. Rev. B*, 2020, **101**, 035144.
93 H. Shinaoka, N. Chikano, E. Gull, J. Li, T. Nomoto, J. Otsuki, M. Wallerberger, T. Wang and K. Yoshimi, Efficient ab initio many-body calculations based on sparse modeling of Matsubara Green's function, *SciPost Physics Lecture Notes*, 2022, **63**, DOI: **10.21468/SciPostPhysLectNotes.63**.
94 J. Fei, C.-N. Yeh, D. Zgid and E. Gull, Analytical continuation of matrix-valued functions: Carathéodory formalism, *Phys. Rev. B*, 2021, **104**, 165111.
95 S. Iskakov, C.-N. Yeh, P. Pokhilko, Y. Yu, L. Zhang, G. Harsha, V. Abraham, M. Wen, M. Wang, J. Adamski, T. Chen, E. Gull and D. Zgid, Green/WeakCoupling: Implementation of fully self-consistent finite-temperature many-body perturbation theory for molecules and solids, *arXiv*, 2024, preprint, arXiv:2406.18479 [cond-mat.mtrl-sci], DOI: **10.48550/arXiv.2406.18479**.
96 P. Becker, P. Scyfried and H. Siegert, The lattice parameter of highly pure silicon single crystals, *Z. Phys. B: Condens. Matter*, 1982, **48**, 17.
97 H. J. McSkimin and P. Andreatch Jr, Elastic Moduli of Silicon vs. Hydrostatic Pressure at 25.0°C and -195.8°C, *J. Appl. Phys.*, 1964, **35**, 2161.
98 O. Brümmer, V. Alex and G. Schulze, Anwendung der Elektronenstrahlmikrosonde für das Weitwinkel-Durchstrahlverfahren, *Ann. Phys.*, 1972, **483**, 118.
99 H. J. McSkimin and P. Andreatch Jr, Elastic Moduli of Germanium versus Hydrostatic Pressure at 25.0°C and -195.8°C, *J. Appl. Phys.*, 1963, **34**, 651.
100 J. Thewlis and A. R. Davey, Thermal Expansion of Grey Tin, *Nature*, 1954, **174**, 1011.
101 C. J. Buchenauer, M. Cardona and F. H. Pollak, Raman Scattering in Gray Tin, *Phys. Rev. B: Solid State*, 1971, **3**, 1243.
102 S. Goedecker, M. Teter and J. Hutter, Separable dual-space Gaussian pseudopotentials, *Phys. Rev. B: Condens. Matter Mater. Phys.*, 1996, **54**, 1703.
103 C. Hartwigsen, S. Goedecker and J. Hutter, Relativistic separable dual-space Gaussian pseudopotentials from H to Rn, *Phys. Rev. B: Condens. Matter Mater. Phys.*, 1998, **58**, 3641.

104 T. Fukumori and K. Futagami, Measurements of Lattice Parameters and Half-Widths of the Rocking Curve on GaAs Crystal by the X-Ray Double-Crystal Method Using a Cu Kα Doublet, *Jpn. J. Appl. Phys.*, 1988, **27**, 442.
105 R. J. Nelmes and M. I. McMahon, Structural Transitions in the Group IV, III-V, and II-VI Semiconductors under Pressure, in *Semiconductors and Semimetals*, ed. T. Suski and W. Paul, Elsevier, 1998, ch. 3, vol. 54, pp. 145–246.
106 C. F. Cline and D. R. Stephens, Volume Compressibility of BeO and Other II-VI Compounds, *J. Appl. Phys.*, 1965, **36**, 2869.
107 J. S. Blakemore, Semiconducting and other major properties of gallium arsenide, *J. Appl. Phys.*, 1982, **53**, R123.
108 J. Pellicer-Porres, D. Martínez-García, C. Ferrer-Roca, A. Segura, V. Muñoz-Sanjosé, J. P. Itié, A. Polian and P. Munsch, High-pressure phase diagram of $ZnSe_xTe_{1-x}$ alloys, *Phys. Rev. B: Condens. Matter Mater. Phys.*, 2005, **71**, 035210.
109 M. E. Straumanis and C. D. Kim, Lattice Parameters, Thermal Expansion Coefficients, Phase Width, and Perfection of the Structure of GaSb and InSb, *J. Appl. Phys.*, 1965, **36**, 3822.
110 T. Kotani and M. van Schilfgaarde, Fusion of the LAPW and LMTO methods: the augmented plane wave plus muffin-tin orbital method, *Phys. Rev. B: Condens. Matter Mater. Phys.*, 2010, **81**, 125117.
111 L. G. Jiao and Y. K. Ho, Application of Löwdin's canonical orthogonalization method to the Slater-type orbital configuration-interaction basis set, *Int. J. Quantum Chem.*, 2015, **115**, 434.
112 F. Karsai, F. Tran and P. Blaha, On the importance of local orbitals using second energy derivatives for d and f electrons, *Comput. Phys. Commun.*, 2017, **220**, 230.
113 G. W. Boggess, J. D. Allen and G. K. Schweitzer, The photoelectron spectra of gaseous zinc(II) and cadmium(II) chlorides, bromides, and iodides, *J. Electron Spectrosc. Relat. Phenom.*, 1973, **2**, 467.
114 J. Eland, Photoelectron spectra and chemical bonding of mercury(II) compounds, *Int. J. Mass Spectrom. Ion Phys.*, 1970, **4**, 37.
115 L. E. Roy, P. J. Hay and R. L. Martin, Revised Basis Sets for the LANL Effective Core Potentials, *J. Chem. Theory Comput.*, 2008, **4**, 1029.
116 M. Burkatzki, C. Filippi and M. Dolg, Energy-consistent small-core pseudopotentials for 3d-transition metals adapted to quantum Monte Carlo calculations, *J. Chem. Phys.*, 2008, **129**, 164115.
117 A. Weigand, X. Cao, T. Hangele and M. Dolg, Relativistic Small-Core Pseudopotentials for Actinium, Thorium, and Protactinium, *J. Phys. Chem. A*, 2014, **118**, 2519.
118 A. Zaitsevskii, N. S. Mosyagin, A. V. Oleynichenko and E. Eliav, Generalized relativistic small-core pseudopotentials accounting for quantum electrodynamic effects: construction and pilot applications, *Int. J. Quantum Chem.*, 2023, **123**, e27077.
119 A. N. Hill, A. J. H. M. Meijer and J. G. Hill, Correlation Consistent Basis Sets and Core Polarization Potentials for Al–Ar with ccECP Pseudopotentials, *J. Phys. Chem. A*, 2022, **126**, 5853.
120 T. H. Dunning Jr, Gaussian basis sets for use in correlated molecular calculations. I. The atoms boron through neon and hydrogen, *J. Chem. Phys.*, 1989, **90**, 1007.

121 J. Heyd, J. E. Peralta, G. E. Scuseria and R. L. Martin, Energy band gaps and lattice parameters evaluated with the Heyd-Scuseria-Ernzerhof screened hybrid functional, *J. Chem. Phys.*, 2005, **123**, 174101.
122 J. Lee, X. Feng, L. A. Cunha, J. F. Gonthier, E. Epifanovsky and M. Head-Gordon, Approaching the basis set limit in Gaussian-orbital-based periodic calculations with transferability: performance of pure density functionals for simple semiconductors, *J. Chem. Phys.*, 2021, **155**, 164102.
123 K. J. Rueda Espinosa, A. A. Kananenka and A. A. Rusakov, Novel Computational Chemistry Infrastructure for Simulating Astatide in Water: From Basis Sets to Force Fields Using Particle Swarm Optimization, *J. Chem. Theory Comput.*, 2023, **19**, 7998.
124 C. Zhang and L. Cheng, Atomic mean-field approach within exact two-component theory based on the Dirac–Coulomb–Breit Hamiltonian, *J. Phys. Chem. A*, 2022, **126**, 4537, pMID: 35763592.
125 H.-Z. Ye and T. C. Berkelbach, Correlation-Consistent Gaussian Basis Sets for Solids Made Simple, *J. Chem. Theory Comput.*, 2022, **18**, 1595.
126 Y. Zhou, E. Gull and D. Zgid, Material-Specific Optimization of Gaussian Basis Sets against Plane Wave Data, *J. Chem. Theory Comput.*, 2021, **17**, 5611.
127 S. Lehtola, Curing basis set overcompleteness with pivoted Cholesky decompositions, *J. Chem. Phys.*, 2019, **151**, 241102.
128 S. Lehtola, Accurate reproduction of strongly repulsive interatomic potentials, *Phys. Rev. A*, 2020, **101**, 032504.
129 S. R. White and E. M. Stoudenmire, Multisliced gausslet basis sets for electronic structure, *Phys. Rev. B*, 2019, **99**, 081110.
130 Y. Qiu and S. R. White, Hybrid gausslet/Gaussian basis sets, *J. Chem. Phys.*, 2021, **155**, 184107.
131 S. R. White and M. J. Lindsey, Nested gausslet basis sets, *J. Chem. Phys.*, 2023, **159**, 234112.
132 N. Jolly, Y. N. Fernández and X. Waintal, Tensorized orbitals for computational chemistry, *arXiv*, 2023, preprint arxiv:2308.03508, 10.48550.